Quartz Crystal Microbalance Gravimetry Measurements of the Sorption of Trimethylaluminum into Polystyrene and Poly(methyl methacrylate)

Emily K. McGuinness⁺, Yifan Liu⁺, Rampi Ramprasad⁺, Mark D. Losego^{+*}

⁺School of Materials Science and Engineering, Georgia Institute of Technology Atlanta, GA 30332

*Corresponding Author: losego@gatech.edu

Abstract

The sorption behavior of metalorganic species into polymers is important in various gas-phase processes including vapor phase infiltration (VPI) which is used to transform organic polymers into organic-inorganic hybrid materials and area-selective deposition where various organic layers are used to prevent vapor deposition. In this work, we use *in situ* quartz crystal microbalance (QCM) gravimetry to measure the long-term mass uptake of TMA into polystyrene (PS) and compare it with that of poly(methyl methacrylate) [PMMA]. While TMA infiltration into PMMA, PS, and PMMA-PS copolymers is widely studied, a direct investigation of TMA's long term sorption behavior into pure PS has not previously been reported. During a 17.5 hour TMA exposure step, PMMA is found to sorb 0.67-0.83 nanograms of TMA per nanogram of polymer while PS is found to sorb only 0.02 nanograms per nanogram polymer. These results clarify that mechanism for low TMA infiltration into PS is a lack of sorption rather than rapid out-diffusion of the precursor. This result has implications ranging from designing impermeable layers for selective area deposition to predicting mass transport in ordered block copolymers. Here, the poor sorption of TMA into PS is utilized in a demonstration to pattern inorganic infiltration into PET films.

Keywords: vapor phase infiltration, quartz crystal microbalance gravimetry, vapor sorption in polymers, trimethylaluminum, polystyrene, poly(methyl methacrylate), area-selective infiltration

1. Introduction:

Vapor phase infiltration (VPI) creates hybrid organic-inorganic materials by incorporating inorganic constituents within polymers via exposure to metalorganic vapor phase precursors and co-reactants. These hybrid materials possess properties distinct from the parent polymer including enhanced mechanical properties, ¹⁻⁶ increased electrical conductivity, ⁷⁻¹⁰ solvent stability, ^{11,12} catalytic capabilities, ¹³ and photoluminescence. ¹³⁻¹⁵ VPI forms these hybrid materials across numerous length scales and without significantly modifying the original polymer's macroscale form factor. As a result, VPI has been used in applications spanning chemical separations ^{12,16-19} to photovoltaics ^{20,21} and more. The capabilities of VPI are the subject of several comprehensive review articles. ²²⁻²⁵

While hybrid organic-inorganic materials created via VPI demonstrate utility for a range of applications, different precursor / polymer systems exhibit vastly different infiltration behaviors. Variations are frequently observed in hybrid material inorganic loadings, inorganic distributions, and chemical states. These behaviors reflect a complex (and often competing) dependence upon

precursor sorption and reaction thermodynamics as well as kinetics. ²⁶ The combination of well infiltrating and poorly infiltrating systems within one structure leads to applications in hybrid material patterning and characterization. When well infiltrating and poorly infiltrating polymers exhibit phase separation within a material (block copolymers, ²⁷⁻³⁴ polymer blends, polymer / small molecule blends³⁵), preferential infiltration into one phase over the other can lead to phase contrast for imaging or inorganic templating applications. For example, block copolymer nanopatterning is utilized to create metal oxide nanostructures from block copolymer templates of generally poorly infiltrating polymers (polystyrene) with well infiltrating polymers (PMMA, ^{19,30,31,36} poly(2-vinylpyridine), ³⁴ etc.). These templated structures have been studied for applications in catalysis, 32 photovoltaics, 37 filtration, 19,38 optoelectric nanomeshes, 34 lithography and pattern transfer, 39-42 and to improve fundamental understanding of block copolymer three dimensional structure by providing phase contrast in electron microscopy. 43 Beyond phase-separation induced templating, area-selective grafting of poorly infiltrating PS brushes has been effective in deactivating surfaces for area-selective vapor deposition of metal oxides. 44 All of these application spaces hinge on the poor infiltration of a specific precursor / polymer system with one of the most common being trimethylaluminum and polystyrene (PS).

Understanding the mechanism behind this lack of infiltration is key to developing advances in the templating of nanostructures (new polymers, thinner materials, etc.) as well as advancing application spaces such as masking and selective area deposition. As a result, several studies have explored the lack of infiltration of various precursors into pure PS films, contrasting this response with well infiltrating polymers. In situ spectroscopic ellipsometry experiments by multiple groups revealed limited swelling (<2%) of PS films during relatively short TMA exposures (1-5 min) at 80, 90, and 120 °C. This in situ data further indicated the infiltration of PS was minimal and did not extend throughout the entire film thickness but was limited to a small portion of the polymer sub-surface. 45,46 Ex situ ellipsometry and SEM characterization of the alumina remaining after removal of PS via plasma revealed a highly porous structure pointing to nucleation and growth of the inorganic at defect sites (such as chain ends) rather than amongst the polymer chains. In this study, it also was found that the introduction of varying quantities of MMA functional groups led to a proportional increase in film swelling and a denser alumina morphology upon the removal of the polymer. 45 In situ FTIR and XPS characterization of PS films infiltrated with TMA for 5 min show no evidence of chemical interactions between TMA and PS and further support a lack of overall TMA uptake. 46 Additional ex situ ellipsometric studies have similarly reported minimal PS film swelling following infiltration with TMA and by TOF-SIMS found VPI treated PS films did not possess strong aluminum signal throughout the ~200 nm of the polymer film. ⁴⁷

From the current body of work, two mechanisms (illustrated in **Figure 1**) have been proposed for the minimal infiltration of PS. In the first mechanism, TMA sorbs significantly within PS, but diffuses out rapidly during a subsequent pumping or purging step (common to most VPI processes). In this mechanism, the lack of strong interactions between precursor and polymer leads to failure in entrapping the precursor within the polymer film^{29,43,45,48} In the second mechanism, the precursor fails to significantly enter the bulk of the polymer during a reasonable timeframe leading to poor infiltration. ^{45,46} The lack of sorption in this mechanism may be due to either slow kinetics or a lack of solubility.

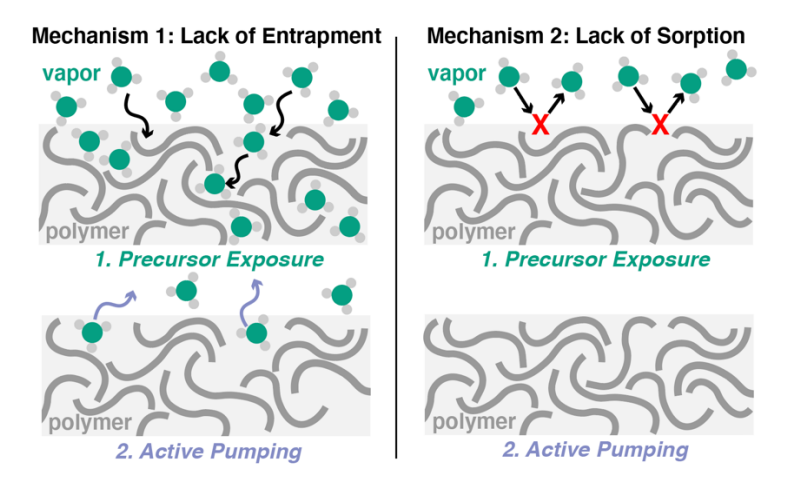


Figure 1. Proposed mechanisms for the poor infiltration of PS with TMA including 1) a lack of precursor entrapment and rapid out-diffusion and 2) a lack of precursor sorption.

In this work, we use QCM gravimetry to explore the mechanism for the low infiltration of TMA into PS at temperatures both above and below the glass transition. The infiltration behavior of PS is compared with that of PMMA under the same infiltration conditions. Using this knowledge, a simple demonstration of area-selective vapor phase infiltration is performed under long TMA exposure infiltration conditions by patterning poly(ethylene terephthalate) [PET] films with a PS coating.

2. Materials and Methods

2.1 Synthesis of Polystyrene and Preparation of Thin Films:

Polystyrene was synthesized via thermally induced free radical polymerization as described in Bamford *et al.* ⁴⁷ and thin films of PS and PMMA (Polysciences, Inc, 75K molecular weight) were spun cast and annealed on Inficon patterned polished gold coated RC cut quartz crystals (Phillip Technologies) as described in McGuinness *et al.* ²⁶ Film thicknesses were measured directly with a J.A. Woollam Alpha-SE spectroscopic ellipsometry employing a Cauchy model.

2.2 In situ Quartz Crystal Microbalance Measurements:

QCM experiments were conducted in a hot-walled custom-built VPI reactor described elsewhere. ²⁶ The wall temperatures and temperature of the sensor holder were set to the same temperature for each experiment (either 70 or 130 °C). Initial polymer masses were measured directly via changes in frequency before and after spin coating via the Sauebrey equation. ²⁶

The PS and PMMA films were then infiltrated at 70 and 130 °C with trimethylaluminum (TMA, **DANGER:** Pyrophoric, Strem Chemicals, 98%, dosed from room temperature) and co-reacted with water vapor dosed from a glass container (DI Water, dosed from room temperature). Chamber pressures were recorded during the infiltrations with a Baratron capacitance manometer and pressure profiles provided in Figure S1. ²⁶

Similar to infiltration procedures outlined in Ren et al., ²⁶ the chamber first underwent a one-hour nitrogen purge followed by 17.5 hours of active pumping at rough vacuum (~30 mTorr) to remove sorbed water and residual solvents. The reactor was then isolated and TMA was dosed into this static environment to pressures between 7 and 14 Torr. The reactor was left in this state for 17.5 hours and then underwent another 17.5 hours of active pumping. The reactor was isolated once more and water vapor introduced at approximately 17.8 Torr of pressure. The reactor was left in this state for 17.5 hours and then a 17.5 hour active pumping step was performed. The final step before removal was a 2-3 hour nitrogen purge.

Crystal frequency was recorded every half second during this time and was exported and converted to mass via the Sauerbrey equation ensuring the change in mass for the entire process (including polymer mass) was less than 5% of the bare crystal frequency. Frequencies had to be corrected during the pumping stages because the low pressure regime impacted the sensor heating and thus crystal frequency, giving artifacts during the active pumping step vs. purging step. To determine this constant value mismatch, the frequency differences between initial purging and pumping (polymer only) and final pumping and purging (hybrid material only) are averaged. This constant value is then added to all pumping regions to correct for the low-pressure artifact. The artifact originates from heating issues in a vacuum environment. Mass changes during infiltration were then divided by the total polymer mass to normalize the data.

2.3 Scanning Electron Microscopy/ Energy Dispersive X-Ray Analysis (SEM/EDX):

Elemental analysis of the post-infiltration films on QCM crystals as well as PS patterned PET films was conducted using a Phenom ProX benchtop scanning electron microscope. For the QCM films, EDX maps were obtained for areas of approximately 0.2 mm² under 5 keV in imaging mode with the backscatter detector.

2.4 Preparation and Infiltration of PS Patterned PET Films:

PET films approximately 0.15 mm in width (McMaster-Carr) were cut into approximately 0.5 inch x 0.5 inch pieces and wiped with isopropanol and then dried with nitrogen prior to patterning with PS. PS as described in Section 2.1 was dissolved in toluene (anhydrous, 99.8%, Sigma-Aldrich) to create a 10 weight percent solution. A piece of Kapton tape was placed on one side of the PET film prior to dip coating in the PS solution. The PET film was placed in the solution for approximately 30 seconds while manually agitated (swirled). The coated PET film was then removed with tweezers and allowed to air dry for one minute (drops at the bottom of the film were gently removed via a wipe). Films were then placed in a watch glass and allowed to dry at least overnight prior to infiltration. The Kapton tape was removed immediately prior to infiltration.

Using a large volume (1 cubic foot) custom-built reactor described in Pyronneau *et al*⁴⁹ and McGuinness *et al*, ¹² infiltration was performed using the metalorganic trimethylaluminum (room temperature, Strem Chemicals, 98%, **DANGER: pyrophoric**) and co-reactant deionized water vapor (room temperature). Similar to procedures outlined in Pyronneau *et al*, ¹² films were placed within the heated reactor (either 70 or 130 °C) and actively pumped under rough vacuum (~30 mTorr) for five hours. The chamber environment was then isolated, and the TMA precursor valve

was opened for 5 s which introduced a TMA pressure of approximately 1 Torr. This static TMA atmosphere was then held constant for five hours. The chamber was pumped again for 5 hours to remove excess TMA and any potential byproducts. 2 to 2.5 Torr of water vapor was then introduced (depending on room temperature) to co-react with the TMA and form the final metal oxide. The chamber was held static with water vapor for 5 hours. The chamber was then pumped for 30 minutes prior to opening the chamber. Pressure profiles for these experiments are provided in Figure S2.

2.5 Computational Methods:

In this work, we used the Vienna Ab Initio Simulation Package (VASP) ^{50,51} for DFT calculations, and the ion-electron interaction was modeled using the project-augmented wave (PAW) potentials. ⁵² The Perdew-Burke-Ernzerh of (PBE) ⁵³ exchange-correlation (XC) function was used to treat the quantum mechanical part of the electron-electron interactions. DF2 dispersion corrections ⁵⁴⁻⁵⁶ were included to adequately handle hydrogen bonding and intermolecular interactions which are critical to this study.

3. Results and Discussion

3.1 Investigating the Sorption of TMA into PMMA and PS

To investigate the infiltration behavior of TMA into PMMA and PS, quartz crystal microbalance (QCM) measurements featuring long TMA exposure times and desorption times (17.5 hours) were employed at 70 and 130 °C (below and above the glass transition temperatures of both polymers). Figure 2a plots the normalized mass uptake (mass uptake / mass polymer) under these conditions (pressure profiles and full QCM measurements with water dose provided in Figure S1). TMA readily sorbs and diffuses into PMMA followed by a gradual continuous increase in mass uptake until the point of desorption. Under these conditions, a larger mass uptake is observed for PMMA at 70 °C than 130 °C (~0.84 and ~0.69 nanograms / nanogram polymer respectively) which is consistent with other QCM literature reports of this infiltration system. ⁵⁷ In stark contrast to the results for PMMA, much less TMA sorbs into the PS films at either 70 or 130 °C (~0.014 and ~0.027 nanograms / nanogram polymer respectively). The mass uptake of TMA within PS (as seen best in the inset of Figure 2a) demonstrates an initial rapid increase for both temperatures. At 70 °C, the uptake reaches a pseudo-steady state within the first hour (periodic increases following this point likely can be attributed to QCM electrical noise). At 130 °C, a slight, but continuous increase is observed over the TMA exposure step with a rate of approximately 0.0006 ng TMA / ng polymer per hour.

During the desorption step (facilitated by actively pumping the chamber), free diffusing species exit the polymer. For PMMA, 0.69 and 0.32 nanograms / nanogram polymer desorb at 70 and 130 °C respectively, leaving behind 0.15 and 0.37 nanograms / nanogram polymer of TMA that is chemically interacting with the polymer. For PS, the small amount of mass uptake that does occur, is seen to remain during the desorption step indicating its permanent residence, likely at defect sites such as chain ends.

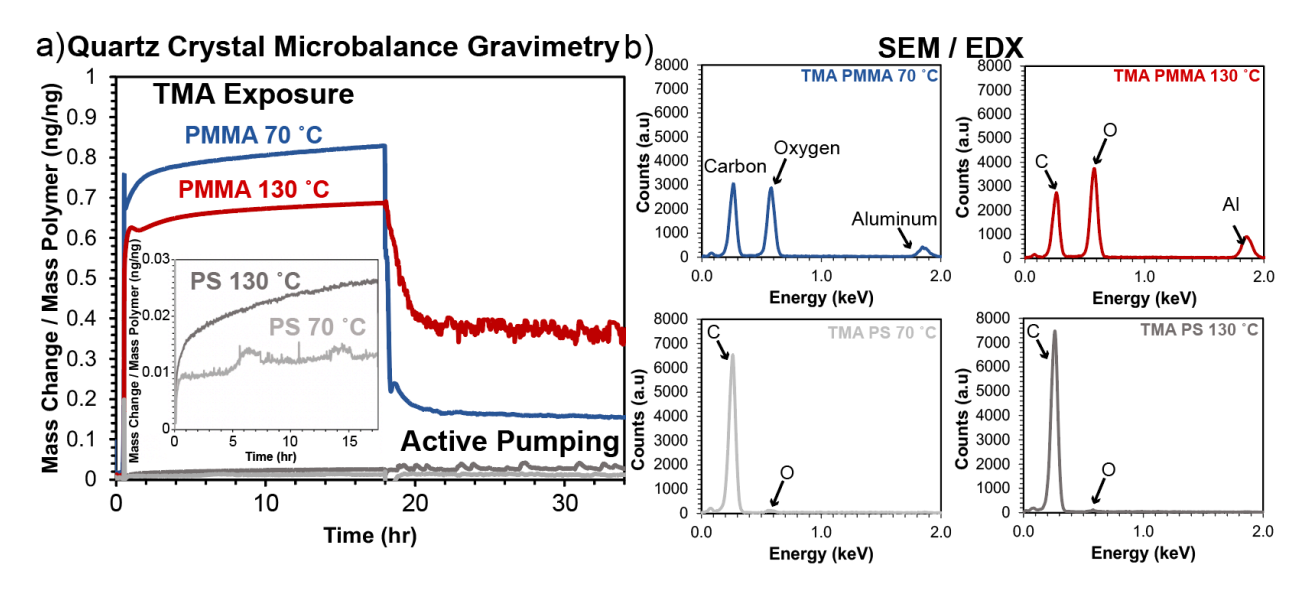


Figure 2. a) Mass uptake versus time plots as generated by *in situ* quartz crystal microbalance measurements during the sorption of TMA into poly(methyl methacrylate) and polystyrene thin films at 70 and 130 °C and subsequent desorption. Inset graph features magnified view of TMA sorption into PS b) *Ex situ* energy dispersive X-Ray spectra for the films in (a).

To verify the lack of infiltration within the PS thin films as compared with PMMA, EDX analysis was performed *ex situ* on the infiltrated polymers via plan-view SEM images approximately 600 by 200 microns in area. The resulting EDX profiles are shown in **Figure 2b**. The profiles of hybrid thin films created via the infiltration of TMA into PMMA demonstrate strong aluminum signal with a greater number of counts of aluminum with respect to carbon for the hybrid thin film created at 130 °C (indicating a larger quantity of inorganic). The profiles of the PS thin films exposed to TMA and water vapor show no identifiable aluminum signal at either 70 or 130 °C, supporting the low infiltration into this system under these conditions.

3.2 Mechanistic Understanding and Insight into the Poor TMA Infiltration into PS

In the literature, two different mechanisms are cited for the poor infiltration of TMA into PS: 1) a lack of reactive functional groups to entrap the precursor within the polymer film^{29,43,45,48} 2) a lack of significant sorption of the precursor into the polymer. ^{45,46} Mechanism 1 supposes that the TMA precursor does sorb and diffuse into the PS, but because PS has no functional groups that react or adduct with TMA, nearly all of the TMA diffuses back out upon removal of the TMA overpressure. However, the QCM measurements in **Figure 2a** reveal little to no mass uptake upon PS exposure to TMA overpressure, strongly refuting mechanism 1. Instead, these QCM results support mechanism 2, that TMA has poor sorption into PS or that TMA is not quickly transported through PS, which has implications ranging from designing impermeable layers for selective area deposition to predicting mass transport in ordered block copolymers.

The low sorption of TMA into PS could have either thermodynamic or kinetic origins. Thermodynamically, solubility depends upon several different chemical and physical factors of both TMA and the polymer including 1) polymer free volume size and connectivity/tortuosity as

compared to precursor size and shape and 2) attractive forces between the precursor and polymer.

Table 1. Glass transition temperatures, fractional free volumes, and oxygen gas permeabilities as predicted by the Polymer Genome Initiative⁵⁸⁻⁶⁰ as well as free volume element radii (measured by PALS⁶¹ and calculated via ROAM⁶²) and Hildebrand Solubility windows from literature and the Polymer Genome Initiative. ^{58,63}

Polymer	Glass Transition Temperature (°C)	Fractional Free Volume	FVE Radius from PALS (Å)	FVE Radius from ROAM (Å)	Oxygen Gas Permeability (Barrer)	Hildebrand Solubility Window (MPa ^{1/2})
PMMA	90 ± 26 K	< 0.18	2.6-2.8	2.6-3.4	0.09	17.4 - 26.7
PS	115 ± 29 K	0.22 ± 0.05	2.8-2.9	2.8-4.0	2.7	17.4 - 21.7

To determine if features of PS free volume are responsible for low TMA solubility, the fractional free volumes, free volume element (FVE) sizes, and oxygen gas permeability coefficients for PS and PMMA are compared in Table 1 and the Van der Waals volume and minimal projection radius for TMA in both monomeric and dimeric forms are provided in **Table 2**. While many polymer free volume features vary with molecular weight and processing, PS generally contains FVE's similar (if not larger) in size and quantity to PMMA. As both PMMA and PS have FVE's similar in size to the minimal projection radius of monomeric TMA (3.4 Å), the physical structure of PS is unlikely to be the primary reason for low TMA sorption. Further, in terms of gas permeability, PS demonstrates a higher permeability for most gases (O2, CO2, He, H2, N2, CH4 as noted on the Polymer Genome Initiative⁵⁸) as compared to PMMA indicating that of the two polymers, PS should be more likely to sorb TMA. The observed change in infiltration behavior for PS above its T_g as compared to its glassy state may indicate a slight dependency on free volume elements and polymer chain mobility. Yet, this change in infiltration behavior for PS above and below Tg is still far from the behaviors observed for PMMA indicating that the initial free volume is not largely responsible for the difference in these systems. We also observe that in terms of the precursor geometry, the slightly larger minimal projection radius of the dimeric form (3.7 Å) may make sorption of the TMA dimer more challenging for both polymers.

Table 2. Precursor Hildebrand solubility parameters calculated via DFT and from literature⁶⁴ along with minimal projection radius and Van der Waals volumes calculated from MarvinSketch.

Precursor	Hildebrand Solubility Parameter from DFT (MPa ^{1/2})	Literature Hildebrand Solubility Parameter (MPa ^{1/2})	Minimal Projection Radius (Å)	Van der Waals Volume (ų) [dimer]
TMA Monomer	30.23	20.8	3.4	84.4
TMA Dimer	-		3.7	152.2

With the physical structure of the polymer an unlikely source of the low TMA sorption into PS, we now explore the role chemical functional groups may play in promoting or preventing precursor sorption. In addition to the experimental results in this work, short-term exposure experimental evidence for the mechanism of TMA sorption into PS, can be found in the in situ spectroscopic ellipsometry works of Caligore et. al. and Cianci et. al. where significant swelling of PMMA films was observed during TMA exposure along with minimal swelling for PS films (both below their Tg). 45,65 The swelling of PMMA films indicates that TMA may plasticize the polymer chains providing flexibility to create additional free volume elements during the infiltration process. The lack of swelling of PS supports the converse. Interestingly, even a small quantity of interacting functional groups (such as MMA or HEMA) when randomly integrated into a PS backbone can dramatically alter sorption behavior. For example, PS-r-PHEMA copolymers with only 3.0% HEMA content result in an almost three-fold increase in inorganic within the film as compared to neat PS films (measured ex situ via spectroscopic ellipsometry following organic removal). ⁴⁷ As a function of interacting functional group content, both HEMA and MMA content have been found to proportionally increase inorganic quantity following VPI with TMA (consistently for MMA and up to 20.2% HEMA). 45,47

Similarly, Kamcev *et al.* found that when the chemical structure of PS-b-PMMA copolymers was altered by UV induced photo-oxidation to produce carbonyl groups within the PS regions (ketones, aldehydes, carboxyl), the infiltration of TMA into PS increased (although not to the level of typical infiltration of TMA within PMMA). Additionally, the PS domains then became selective to infiltration with additional precursors, DEZ and titanium isopropoxide. ²⁹ In the context of these literature results, it is evident that a small quantity of interactive functional groups significantly alters the sorption characteristics of PS highlighting the imperative role that interactive functional groups play in not only the entrapment processes of VPI, but also in the sorption of the precursor. Additionally, once a precursor infiltrates within a polymer and even possibly reacts, the presence of the entrapped precursor may facilitate additional sorption.

These literature results in addition to the experiments in this work highlight the importance of chemical functionality which controls both thermodynamic principles such as precursor / polymer solubility and kinetic principles such as facilitated transport mechanisms.

Thermodynamically, good solubility represents a low enthalpy of mixing between the sorbing molecule and the polymer which results from similar cohesive energies ("like dissolves like"). Frameworks for quantifying these interactions and predicting polymer solubilities are an ongoing area of study. ⁶⁶ One frequently used framework for understanding solubility is the Hildebrand solubility parameter. The Hildebrand solubility parameter (δ) represents a material's total cohesive interactions and is related to the enthalpy of vaporization (H_V) and molar volume (V) of the molecule through *Equation 2*.

$$\delta = \left(\frac{H_v - RT}{V}\right)^{0.5} \tag{Equation 2}$$

For solvents and other small molecules with observable boiling points, these values can be calculated; however, polymers generally degrade before reaching the point of vaporization. Therefore, their Hildebrand solubility parameters are estimated by evaluating polymer solubility

in a range of solvents with known solubility parameters and approximating the parameter from the results. Additional methods for determining the solubility of a polymer include group contribution theory, ⁶⁷ density functional theory, and machine learning based on available experimental datasets. ⁶⁶ The Hildebrand solubility windows of PMMA and PS as computed in the Polymer Genome Initiative⁵⁸ and experimentally determined in literature⁶³ are presented in Table 1. The Hildebrand solubility windows of PMMA and PS are 17.4 - 26.7 and 17.4 - 21.7 respectively. While these solubility parameters are different enough to cause phase separation of block copolymers made of these two polymers, they are similar enough in value that PMMA and PS share many common solvents. The Hildebrand solubility parameter for TMA from literature and as computed through DFT is presented in **Table 2**. In literature⁶⁴ the experimentally reported Hildebrand solubility parameter for TMA is 20.8 MPa^{1/2}, which differs significantly from the Hildebrand solubility parameter that we computed from DFT using cohesion energies (30.2 MPa^{1/2}). The difference between the computed value and the experimental may be due to TMA frequently existing in a dimeric form rather than the monomer form used for DFT or that the cohesion energy calculated relies upon starting in crystallographic form rather than liquid form (which TMA exists as at the experimental temperature).

While the experimental solubility parameter of TMA is within the Hildebrand solubility window of both polymers and the DFT computed parameter is outside of both, we speculate that the significantly wider solubility window of PMMA leads to improved solubility of TMA into PMMA. Taking this solubility window approach, we hypothesize that differences in solubility driven by cohesive energy differences may explain the different TMA sorption behavior for these two polymers. Additionally, DFT results from literature support significantly different interactions between the polymers and TMA with the stabilization energy of TMA with PMMA found to be 14.17 kcal/mol and TMA with PS as -2.66 kcal/mol. 68

In addition to modifying the thermodynamic solubility behavior, functional groups may also facilitate faster transport mechanisms for the precursor within the polymer. The 17.5 h exposure time utilized herein does not constitute an infinite hold time and the uptake of TMA into PS, especially at 130 °C, may continue to increase over longer times. In polymer membrane literature, the presence of functional groups that bind and debind with a diffusing molecule can improve the rate of diffusion through a facilitated transport mechanism. ⁶⁹ In fact, this mechanism has been proposed and both experimentally and computationally supported for VPI in work by Sasao *et al.* ^{68,70} Therefore, a lack of facilitated transport may also play a role in the behavior of TMA sorption into PS.

From these findings, the mechanism of low TMA infiltration into PS is specified to one of low sorption arising from chemical rather than physical aspects of the polymer. However, the exact role of chemical functionality in this infiltration process is still unclear and may be thermodynamic, kinetic, or a combination as functional groups control both solubility and transport mechanisms.

3.3 Utilizing PS as an Infiltration Blocking Layer or For Area Selective Infiltration

As a final demonstration of PS's ability to block TMA mass transport, poly(ethylene terephthalate) [PET] films were spatially coated with PS and then infiltrated with TMA and water vapor at 70

and 130 °C. PET is known to infiltrate rapidly and to a large extent with TMA at both of these temperatures with a known color change above 100 °C. ^{13,14,49} As shown in **Figure 3a**, approximately 0.15 mm thick PET films were coated with PS by dip coating in a 10 weight percent solution of PS in toluene. Patterned films were created by attaching Kapton tape to one side of the film prior to dip coating which was removed immediately prior to infiltration featuring a five h TMA exposure step as described in Section 2.4.

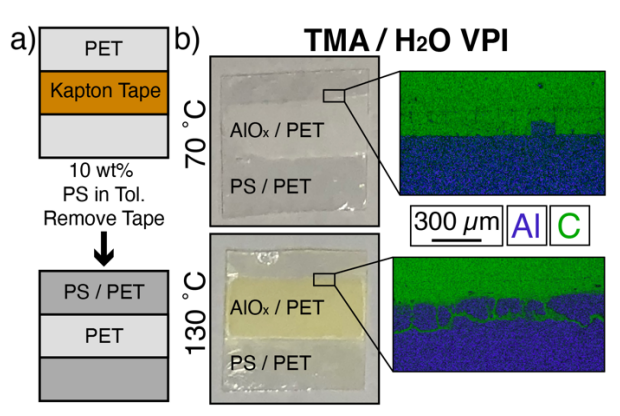


Figure 3. Vapor phase infiltration of PS patterned PET films. a) Preparation of \sim 0.15 mm thick PET patterned with a coating of \sim 2-4 micron thick PS by masking with Kapton tape and dip coating in 10 weight percent PS in toluene. b) Photographs of patterned PS / PET films after infiltration with trimethylaluminum and water vapor at 70 and 130 °C accompanied by SEM / EDX at higher magnifications.

Figure 3b shows photographs taken of the PS patterned PET films following infiltration. For both infiltration temperatures, the portion of the film that was not coated with PS turns hazy and is white at 70 °C and yellow at 130 °C while the portions that are coated with PS remain colorless and clear. To confirm selective infiltration with aluminum, SEM images with EDX maps were taken (in plan view) of the edges of the patterned regions which reveal significant aluminum presences in the patterned regions alone. Cross section SEM images with EDX maps in **Figure S3** demonstrate aluminum signal into the bulk of uncoated PET films and no aluminum signal within the bulk of PS coated PET.

These results emphasize experimentally the utility of non-infiltrating for patterning applications even through simple methods such as selective polymer coating from solution. Further, the patterning behavior highlights how PS coatings under these conditions can serve as an effective blocking layer even during long exposure times by preventing TMA from reaching the underlying substrate. Ultimately, this patterning is possible because the poor infiltration of TMA into PS is the result of minimal sorption rather than significant sorption with no entrapment.

Conclusions

QCM gravimetry has been used to study the sorption of TMA into PS and PMMA above and below their glass transition temperatures. As expected, PMMA sorbs a large amount of TMA. Interestingly, though, PS sorbs near zero TMA precursor. The low sorption of TMA into PS reveals that the lack of TMA infiltration into PS is a result of poor sorption and not just a lack of binding

interactions within the bulk of the polymer. This lack of sorption does not appear to be the result of differences in free volume of the polymers but rather likely related to a lack of chemically interacting functional groups that minimize overall thermodynamic sorption and/or facilitated transport. This highlights the significant role that functional groups play in VPI beyond mechanisms for chemical entrapment. Polystyrene's effective blocking of TMA sorption has significant implications for area-selective patterning. Here we conduct a proof-of-concept demonstration of area-selective infiltration using simple selective PS coatings on PET films during long TMA exposures. An improved understanding of the chemical mechanisms that limit and/or enhance sorption of inorganic precursors into a polymer will advance new pathways to area-selective deposition. Moreover, this understanding will have direct implications to the kinetics of vapor infiltration into self-assembled block-copolymer structures; if precursors do not enter certain polymer blocks, this will increase tortuosity and reduce overall transport kinetics.

Acknowledgements

E.K.M. was supported in part by the Department of Defense (DoD) through the National Defense Science & Engineering Graduate (NDSEG) Fellowship Program. E.K.M., Y.L, R.R., M.D.L. also received support from the National Science Foundation (DMREF-1921873). Part of this research was conducted in Georgia Tech's Materials Innovation & Learning Laboratory (The MILL), an uncommon "make and measure" space committed to elevating undergraduate research in materials science. The authors are grateful to Ronald A. Smith and Professor Will R. Gutekunst from the School of Chemistry and Biochemistry at the Georgia Institute of Technology for the synthesis of the polystyrene used in this work.

REFERENCES

- Lee, S. M. *et al.* Greatly increased toughness of infiltrated spider silk. *Science* **324**, 488-492, doi:10.1126/science.1168162 (2009).
- Sun, Y. J. *et al.* Influence of Subsurface Hybrid Material Growth on the Mechanical Properties of Atomic Layer Deposited Thin Films on Polymers. *Chemical Vapor Deposition* **19**, 134-141, doi:10.1002/cvde.201207042 (2013).
- Dusoe, K. J. *et al.* Ultrahigh Elastic Strain Energy Storage in Metal-Oxide-Infiltrated Patterned Hybrid Polymer Nanocomposites. *Nano Lett* **17**, 7416-7423, doi:10.1021/acs.nanolett.7b03238 (2017).
- 4 Lee, S.-M. *et al.* In Situ Raman Spectroscopic Study of Al-Infiltrated Spider Dragline Silk under Tensile Deformation. *ACS Appl. Mater. Interfaces* **6**, 16827-16834, doi:10.1021/am5041797 (2014).
- McClure, C. D., Oldham, C. J. & Parsons, G. N. Effect of Al2O3 ALD coating and vapor infusion on the bulk mechanical response of elastic and viscoelastic polymers. *Surface & Coatings Technology* **261**, 411-417, doi:10.1016/j.surfcoat.2014.10.029 (2015).
- Padbury, R. P. & Jur, J. S. Systematic study of trimethyl aluminum infiltration in polyethylene terephthalate and its effect on the mechanical properties of polyethylene terephthalate fibers. *J Vac Sci Technol A* **33**, 9, doi:Artn 01a112

10.1116/1.4898435 (2015).

- Wang, W. et al. Conductive Polymer-Inorganic Hybrid Materials through Synergistic Mutual Doping of the Constituents. ACS Appl Mater Interfaces 9, 27964-27971, doi:10.1021/acsami.7b09270 (2017).
- Wang, W. *et al.* Efficient and controllable vapor to solid doping of the polythiophene P3HT by low temperature vapor phase infiltration. *J. Mater. Chem. C* **5**, 2686-2694, doi:10.1039/c6tc05544c (2017).
- 9 Wang, W. K. *et al.* Tuning the Conductivity of Polyaniline through Doping by Means of Single Precursor Vapor Phase Infiltration. *Adv. Mater. Interfaces* **4**, 1600806-1600806, doi:ARTN 1600806

10.1002/admi.201600806 (2017).

- Gregory, S. A. *et al.* Vapor Phase Infiltration Doping of the Semiconducting Polymer Poly(aniline) with TiCl4 + H2O: Mechanisms, Reaction Kinetics, and Electrical and Optical Properties. *ACS Applied Polymer Materials* **3**, 720-729, doi:10.1021/acsapm.0c01014 (2021).
- McGuinness, E. K., Leng, C. Z. & Losego, M. D. Increased Chemical Stability of Vapor-Phase Infiltrated AlOx-Poly(methyl methacrylate) Hybrid Materials. *Acs Applied Polymer Materials* **2**, 1335-1344, doi:10.1021/acsapm.9b01207 (2020).
- McGuinness, E. K., Zhang, F. Y., Ma, Y., Lively, R. P. & Losego, M. D. Vapor Phase Infiltration of Metal Oxides into Nanoporous Polymers for Organic Solvent Separation Membranes. *Chem. Mat.* **31**, 5509-5518, doi:10.1021/acs.chemmater.9b01141 (2019).
- Akyildiz, H. I., Stano, K. L., Roberts, A. T., Everitt, H. O. & Jur, J. S. Photoluminescence Mechanism and Photocatalytic Activity of Organic-Inorganic Hybrid Materials Formed by Sequential Vapor Infiltration. *Langmuir* **32**, 4289-4296, doi:10.1021/acs.langmuir.6b00285 (2016).
- Akyildiz, H. I. *et al.* Formation of novel photoluminescent hybrid materials by sequential vapor infiltration into polyethylene terephthalate fibers. *J. Mater. Res.* **29**, 2817-2826, doi:10.1557/jmr.2014.333 (2014).

Akyildiz, H. I., Mousa, M. B. M. & Jur, J. S. Atmospheric pressure synthesis of photoluminescent hybrid materials by sequential organometallic vapor infiltration into polyethylene terephthalate fibers. *J. Appl. Phys.* **117**, 7, doi:Artn 045301

10.1063/1.4906406 (2015).

- Bergsman, D. S., Getachew, B. A., Cooper, C. B. & Grossman, J. C. Preserving nanoscale features in polymers during laser induced graphene formation using sequential infiltration synthesis. *Nat Commun* **11**, 3636, doi:10.1038/s41467-020-17259-5 (2020).
- 17 Chen, X. *et al.* Tailoring the Microporosity of Polymers of Intrinsic Microporosity for Advanced Gas Separation by Atomic Layer Deposition. *Angewandte Chemie International Edition* **60**, 17875-17880, doi:https://doi.org/10.1002/anie.202016901 (2021).
- Waldman, R. Z. *et al.* Sequential Infiltration Synthesis of Al2O3 in Polyethersulfone Membranes. *Jom* **71**, 212-223, doi:10.1007/s11837-018-3142-3 (2019).
- Zhou, C. *et al.* Fabrication of Nanoporous Alumina Ultrafiltration Membrane with Tunable Pore Size Using Block Copolymer Templates. *Adv Funct Mater* **27**, 1701756, doi:https://doi.org/10.1002/adfm.201701756 (2017).
- Nahor, O., Segal-Peretz, T., Neeman, L., Oron, D. & Frey, G. L. Controlling morphology and charge transfer in ZnO/polythiophene photovoltaic films. *J. Mater. Chem. C* **2**, 4167-4176, doi:10.1039/c3tc32246g (2014).
- Obuchovsky, S. *et al.* Atomic layer deposition of zinc oxide onto and into P3HT for hybrid photovoltaics. *J. Mater. Chem. C* **2**, 8903-8910, doi:10.1039/c4tc01629g (2014).
- Ashurbekova, K., Ashurbekova, K., Botta, G., Yurkevich, O. & Knez, M. Vapor phase processing: a novel approach for fabricating functional hybrid materials. *Nanotechnology* **31**, 342001, doi:10.1088/1361-6528/ab8edb (2020).
- Azpitarte, I. & Knez, M. Vapor phase infiltration: from a bioinspired process to technologic application, a prospective review. *Mrs Communications* **8**, 727-741, doi:10.1557/mrc.2018.126 (2018).
- Leng, C. Z. & Losego, M. D. Vapor phase infiltration (VPI) for transforming polymers into organic-inorganic hybrid materials: a critical review of current progress and future challenges. *Mater. Horizons* **4**, 747-771, doi:10.1039/c7mh00196g (2017).
- Waldman, R. Z. *et al.* The chemical physics of sequential infiltration synthesis-A thermodynamic and kinetic perspective. *J Chem Phys* **151**, 190901, doi:10.1063/1.5128108 (2019).
- Ren, Y. *et al.* Reaction–Diffusion Transport Model to Predict Precursor Uptake and Spatial Distribution in Vapor-Phase Infiltration Processes. *Chem. Mat.* **33**, 5210-5222, doi:10.1021/acs.chemmater.1c01283 (2021).
- Azoulay, R., Shomrat, N., Weisbord, I., Atiya, G. & Segal-Peretz, T. Metal Oxide Heterostructure Array via Spatially Controlled-Growth within Block Copolymer Templates. *Small* **15**, e1904657, doi:10.1002/smll.201904657 (2019).
- Berman, D. & Shevchenko, E. Design of functional composite and all-inorganic nanostructured materials via infiltration of polymer templates with inorganic precursors. *J. Mater. Chem. C* **8**, 10604-10627, doi:10.1039/d0tc00483a (2020).
- Kamcev, J. *et al.* Chemically enhancing block copolymers for block-selective synthesis of self-assembled metal oxide nanostructures. *ACS Nano* **7**, 339-346, doi:10.1021/nn304122b (2013).
- Peng, Q., Tseng, Y. C., Darling, S. B. & Elam, J. W. A route to nanoscopic materials via sequential infiltration synthesis on block copolymer templates. *ACS Nano* **5**, 4600-4606, doi:10.1021/nn2003234 (2011).

- Peng, Q. *et al.* Effect of Nanostructured Domains in Self-Assembled Block Copolymer Films on Sequential Infiltration Synthesis. *Langmuir* **33**, 13214-13223, doi:10.1021/acs.langmuir.7b02922 (2017).
- She, Y. *et al.* Block-Co-polymer-Assisted Synthesis of All Inorganic Highly Porous Heterostructures with Highly Accessible Thermally Stable Functional Centers. *ACS Appl. Mater. Interfaces* **11**, 30154-30162, doi:10.1021/acsami.9b09991 (2019).
- She, Y. *et al.* Effect of the Micelle Opening in Self-assembled Amphiphilic Block Co-polymer Films on the Infiltration of Inorganic Precursors. *Langmuir* **35**, 796-803, doi:10.1021/acs.langmuir.8b04039 (2019).
- Subramanian, A. *et al.* Three-dimensional electroactive ZnO nanomesh directly derived from hierarchically self-assembled block copolymer thin films. *Nanoscale* **11**, 9533-9546, doi:10.1039/c9nr00206e (2019).
- Obuchovsky, S., Levin, M., Levitsky, A. & Frey, G. L. Morphology visualization of P3HT:Fullerene blends by using subsurface atomic layer deposition. *Organic Electronics* **49**, 234-241, doi:https://doi.org/10.1016/j.orgel.2017.06.050 (2017).
- Tseng, Y. C., Peng, Q., Ocola, L. E., Elam, J. W. & Darling, S. B. Enhanced Block Copolymer Lithography Using Sequential Infiltration Synthesis. *Journal of Physical Chemistry C* **115**, 17725-17729, doi:10.1021/jp205532e (2011).
- Allen, J. E. *et al.* Self-assembly of single dielectric nanoparticle layers and integration in polymer-based solar cells. *Applied Physics Letters* **101**, 063105, doi:10.1063/1.4744928 (2012).
- Greil, S., Rahman, A., Liu, M. & Black, C. T. Gas Transport Selectivity of Ultrathin, Nanoporous, Inorganic Membranes Made from Block Copolymer Templates. *Chem. Mat.* **29**, 9572-9578, doi:10.1021/acs.chemmater.7b04174 (2017).
- Tseng, Y.-C., Mane, A. U., Elam, J. W. & Darling, S. B. Enhanced Lithographic Imaging Layer Meets Semiconductor Manufacturing Specification a Decade Early. *Advanced Materials* **24**, 2608-2613, doi:https://doi.org/10.1002/adma.201104871 (2012).
- Ruiz, R. *et al.* Image quality and pattern transfer in directed self assembly with block-selective atomic layer deposition. *Journal of Vacuum Science & Technology B* **30**, 06F202, doi:10.1116/1.4758773 (2012).
- Sunday, D. F. *et al.* Template–polymer commensurability and directed self-assembly block copolymer lithography. *Journal of Polymer Science Part B: Polymer Physics* **53**, 595-603, doi:https://doi.org/10.1002/polb.23675 (2015).
- 42 Doerk, G. S. et al. Transfer of self-aligned spacer patterns for single-digit nanofabrication.
- Segal-Peretz, T. *et al.* Characterizing the Three-Dimensional Structure of Block Copolymers via Sequential Infiltration Synthesis and Scanning Transmission Electron Tomography. *ACS Nano* **9**, 5333-5347, doi:10.1021/acsnano.5b01013 (2015).
- Snelgrove, M. *et al.* Analysing trimethylaluminum infiltration into polymer brushes using a scalable area selective vapor phase process. *Materials Advances* **2**, 769-781, doi:10.1039/D0MA00928H (2021).
- Caligiore, F. E. *et al.* Effect of the Density of Reactive Sites in P(S-r-MMA) Film during Al2O3 Growth by Sequential Infiltration Synthesis. *Adv. Mater. Interfaces* **6**, 1900503-1900503, doi:10.1002/admi.201900503 (2019).
- Petit, R. R. *et al.* Atomic Layer Deposition on Polymer Thin Films: On the Role of Precursor Infiltration and Reactivity. *ACS Appl. Mater. Interfaces* **13**, 46151-46163, doi:10.1021/acsami.1c12933 (2021).
- Bamford, J. T., Smith, R. A., Leng, C. Z., Gutekunst, W. R. & Losego, M. D. Measuring the Glass Transition Temperature of Vapor-Phase-Infiltrated AlOx-PS-r-PHEMA Organic—Inorganic Hybrid Thin-Film Materials. *Macromolecules* **54**, 6790-6798, doi:10.1021/acs.macromol.1c00691 (2021).

- Elam, J. W. *et al.* New Insights into Sequential Infiltration Synthesis. *ECS Transactions* **69**, 147-157, doi:10.1149/06907.0147ecst (2015).
- Pyronneau, K. *et al.* Wash Fastness of Hybrid AlOx-PET Fabrics Created via Vapor-Phase Infiltration. *ACS Applied Polymer Materials*, doi:10.1021/acsapm.1c01851 (2022).
- Kresse G Fau Hafner, J. & Hafner, J. Ab initio molecular dynamics for liquid metals.
- Kresse, G. & Furthmüller, J. Efficiency of ab-initio total energy calculations for metals and semiconductors using a plane-wave basis set. *Computational Materials Science* **6**, 15-50, doi:https://doi.org/10.1016/0927-0256(96)00008-0 (1996).
- Kresse, G. & Joubert, D. From ultrasoft pseudopotentials to the projector augmented-wave method. *Physical Review B* **59**, 1758-1775, doi:10.1103/PhysRevB.59.1758 (1999).
- Perdew Jp Fau Burke, K., Burke K Fau Ernzerhof, M. & Ernzerhof, M. Generalized Gradient Approximation Made Simple.
- Lee, K., Murray, É. D., Kong, L., Lundqvist, B. I. & Langreth, D. C. Higher-accuracy van der Waals density functional. *Physical Review B* **82**, 081101, doi:10.1103/PhysRevB.82.081101 (2010).
- Woods, L. M. *et al.* Materials perspective on Casimir and van der Waals interactions. *Reviews of Modern Physics* **88**, 045003, doi:10.1103/RevModPhys.88.045003 (2016).
- Liu, C.-S., Pilania, G., Wang, C. & Ramprasad, R. How Critical Are the van der Waals Interactions in Polymer Crystals? *The Journal of Physical Chemistry A* **116**, 9347-9352, doi:10.1021/jp3005844 (2012).
- Weisbord, I., Shomrat, N., Azoulay, R., Kaushansky, A. & Segal-Peretz, T. Understanding and Controlling Polymer-Organometallic Precursor Interactions in Sequential Infiltration Synthesis. *Chem. Mat.* **32**, 4499-4508, doi:10.1021/acs.chemmater.0c00026 (2020).
- Doan Tran, H. *et al.* Machine-learning predictions of polymer properties with Polymer Genome. *J. Appl. Phys.* **128**, 171104, doi:10.1063/5.0023759 (2020).
- Huan, T. D. *et al.* A polymer dataset for accelerated property prediction and design. *Scientific Data* **3**, 160012, doi:10.1038/sdata.2016.12 (2016).
- Kim, C., Chandrasekaran, A., Huan, T. D., Das, D. & Ramprasad, R. Polymer Genome: A Data-Powered Polymer Informatics Platform for Property Predictions. *The Journal of Physical Chemistry C* **122**, 17575-17585, doi:10.1021/acs.jpcc.8b02913 (2018).
- Yampolskii, Y. P. Methods for investigation of the free volume in polymers. *Russian Chemical Reviews* **76**, 59-78, doi:10.1070/rc2007v076n01abeh003629 (2007).
- Fica-Contreras, S. M., Hoffman, D. J., Pan, J., Liang, C. & Fayer, M. D. Free Volume Element Sizes and Dynamics in Polystyrene and Poly(methyl methacrylate) Measured with Ultrafast Infrared Spectroscopy. *J. Am. Chem. Soc.* **143**, 3583-3594, doi:10.1021/jacs.0c13397 (2021).
- Gaikwad, A. M. *et al.* Identifying orthogonal solvents for solution processed organic transistors. *Organic Electronics* **30**, 18-29, doi:https://doi.org/10.1016/j.orgel.2015.12.008 (2016).
- House, J. E. Molecular association in trialkylaluminum and alkylaluminum chloride compounds determined from solubility parameters and related thermodynamic quantities. *Journal of Organometallic Chemistry* **263**, 267-271, doi:https://doi.org/10.1016/0022-328X(84)85031-7 (1984).
- 65 Cianci, E., Nazzari, D., Seguini, G. & Perego, M. Trimethylaluminum Diffusion in PMMA Thin Films during Sequential Infiltration Synthesis: In Situ Dynamic Spectroscopic Ellipsometric Investigation. *Adv. Mater. Interfaces* **5**, 1801016-1801016, doi:ARTN 1801016

10.1002/admi.201801016 (2018).

Venkatram, S., Kim, C., Chandrasekaran, A. & Ramprasad, R. Critical Assessment of the Hildebrand and Hansen Solubility Parameters for Polymers. *Journal of Chemical Information and Modeling* **59**, 4188-4194, doi:10.1021/acs.jcim.9b00656 (2019).

- Sheldon, T. J., Adjiman, C. S. & Cordiner, J. L. Pure component properties from group contribution: Hydrogen-bond basicity, hydrogen-bond acidity, Hildebrand solubility parameter, macroscopic surface tension, dipole moment, refractive index and dielectric constant. *Fluid Phase Equilib.* **231**, 27-37, doi:https://doi.org/10.1016/j.fluid.2004.12.017 (2005).
- Sasao, N., Sugimura, S. & Asakawa, K. Polymer designs for dense metal infiltration for higher dryetch resistance. *Japanese Journal of Applied Physics* **59**, SIICO2, doi:10.35848/1347-4065/ab86dd (2020).
- Rea, R., De Angelis, M. G. & Baschetti, M. G. Models for Facilitated Transport Membranes: A Review. *Membranes* **9**, doi:10.3390/membranes9020026 (2019).
- Sasao, N., Sugimura, S. & Asakawa, K. Metal diffusion model in polymer matrices in vapor phase infiltration. *Japanese Journal of Applied Physics* **60**, SCCC04, doi:10.35848/1347-4065/abf2d7 (2021).